Application of De-silylation Strategies to the Preparation of Transition Metal Pnictide Nanocrystals: The Case of FeP

Susanthri C. Perera,[†] Petru S. Fodor,[‡] Georgy M. Tsoi,[‡] Lowell E. Wenger,[‡] and Stephanie L. Brock*,[†]

Departments of Chemistry and Physics & Astronomy, Wayne State University, Detroit, Michigan 48202

Received June 3, 2003. Revised Manuscript Received July 18, 2003

Phase-pure FeP nanoparticles have been synthesized by the reaction of iron(III) acetylacetonate with tris(trimethylsilyl)phosphine at temperatures of 240−320 °C using trioctylphosphine oxide as a solvent and dodecylamine (DA), myristic acid (MA), or hexylphosphonic acid (HPA) as additional capping groups (ligands). The DA-capped particles prepared at 260 °C have an average diameter of 4.65 ± 0.74 nm with FeP being the only observed crystalline phase. Elemental analyses indicate a high percentage yield of FeP (85%) and are consistent with 12% TOPO incorporation in the product. The addition of MA has results similar to those of the addition of DA, whereas addition of HPA seems to inhibit crystallite growth, resulting in very small (ca. 1 nm) or amorphous particles that are difficult to isolate. Magnetic susceptibility data on DA-capped FeP suggest that the moments within each particle are coupled antiferromagnetically, at least over a short range; however, there is no evidence of a Néel transition, in contrast to bulk FeP. It is likely that the FeP particles produced by this route are too small (ca. 5 nm) relative to the magnetic cell (2.9 nm) for the onset of long-range helical antiferromagnetic order, even at low temperatures (5 K) and fields (0.010 T).

Introduction

Since the discovery of size-dependent physical properties for materials with length scales of ≤100 nm,[1] extensive effort has been focused on synthetic methods for the production of discrete, single-phase nanoparticles with low polydispersities. Current methodologies based on arrested precipitation reactions in coordinating solvents or reverse micelles have facilitated the study of nanoparticles from both fundamental and technological viewpoints.[2] These include Si, Ge,[3,4] II−VI (CdSe, CdS),[5−7] and III−V (GaAs, InP)[8,9] semiconductors; and magnetic materials based on elements (Co, Fe),[10,11] alloys (FePt),[12] or oxides (Mn_3O_4, Fe_2O_3).[13,14]

To date, property−size relationships among the transition metal pnictides (pnicogen = Group 15 element) remain uncharted, despite the fact that a number of these materials in bulk form exhibit behaviors ranging from semiconducting to ferromagnetic with technologically relevant magneto-elastic and magneto-optical properties.[15] Thus, synthetic strategies need to be developed that will be appropriate for the synthesis of a variety of transition metal pnictides as discrete nanoparticles and allow for the targeting of specific phases and stoichiometries.

The de-silylation route, which has been employed previously for main group pnictide nanoparticles, employs reactive phosphines and arsines such as $Pn(SiMe_3)_3$ (Pn = P, As) and metal salts (eq 1).

$$MX_3 + Pn(SiMe_3)_3 \rightarrow MPn_{nano} + 3\ XSiMe_3 \quad (MX_3 = \text{trivalent metal salt; Pn = pnicogen}) \quad (1)$$

This strategy is potentially advantageous for transition metal pnictides because it is formally nonredox, and therefore permits, in theory, the targeting of particular phases by controlling the oxidation state of the transi-

* To whom correspondence should be addressed. E-mail: sbrock@chem.wayne.edu.
[†] Department of Chemistry.
[‡] Department of Physics & Astronomy.

(1) (a) Pileni, M. P. *J. Phys. Chem.* **1993**, *97*, 6961−6973. (b) Leslie-Pelecky, D. L.; Rieke, R. D. *Chem. Mater.* **1996**, *8*, 1770−1783.
(2) Rossetti, R.; Nakahara, S.; Brus, L. E. *J. Chem. Phys.* **1983**, *79*, 1086−1088. (b) Alivisatos, A. P. *J. Phys. Chem.* **1996**, *100*, 13226−13239.
(3) Senter, R. A.; Chen, Y.; Coffer, J. L. *Nano Lett.* **2001**, *1*, 383−386. (b) Baldwin, R. K.; Pettigrew, K. A.; Garno, J. C.; Power, P. P.; Liu, G. Y.; Kauzlarich, S. M. *J. Am. Chem. Soc.* **2002**, *124*, 1150−1151.
(4) Taylor, B. R.; Delgado, G. R.; Lee, H. W. H.; Kauzlarich, S. M. *Chem. Mater.* **1999**, *11*, 2493−2500.
(5) Peng, Z. A.; Peng, X. J. *J. Am. Chem. Soc.* **2001**, *123*, 183−184.
(6) Murray, C. B.; Norris, D. J.; Bawendi, M. G. *J. Am. Chem. Soc.* **1993**, *115*, 8706−8715.
(7) Talapin, D. V.; Rogach, A. L.; Kornowski, A.; Haase, M.; Weller, H. *Nano Lett.* **2001**, *1*, 207−211.
(8) Mićić, O. I.; Sprague, R. J.; Curtis, C. J.; Jones, K. M.; Machol, J. L.; Nozik, A. J. *J. Phys. Chem.* **1994**, *98*, 4966−4969.
(9) Guzelian, A. A.; Katari, J. E. B.; Kadavanich, A. V.; Banin, U.; Hamad, K.; Juban, E.; Alivisatos, A. P.; Wolters, R. H.; Arnold, C. C.; Heath, J. R. *J. Phys. Chem.* **1996**, *100*, 7212−7219.
(10) Puntes, V. F.; Krishnan, K. M.; Alivisatos, A. P. *Science* **2001**, *291*, 2115−2117.
(11) Park, S.; Kim, S.; Lee, S.; Khim, Z. G.; Char, K.; Hyeon, T. *J. Am. Chem. Soc.* **2000**, *122*, 8581−8582.
(12) Murray, C. B.; Weller, D.; Folks, L.; Moser, A.; Sun, S. *Science* **2000**, *287*, 1989−1992.
(13) Ocaña, M. *Colloid Polym. Sci.* **2000**, *278*, 443−449.
(14) Feltin, N.; Pileni, M. P. *Langmuir* **1997**, *13*, 3927−3933.
(15) Hulliger, F. *Struct. Bonding* **1968**, *4*, 83−85.

10.1021/cm034443o CCC: $25.00
Published on Web 09/24/2003

tion metal precursor (i.e., $M^{2+} + Pn^{3-} \rightarrow M_3Pn_2$; $M^{3+} + Pn^{3-} \rightarrow MPn$). Because of their rich and complex composition diagrams, such oxidation state control is essential if single-phase, stoichiometrically controlled transition metal pnictide nanoparticles are to be prepared. Accordingly, we have set out to test the applicability of de-silylation routes to transition metal pnictide nanoparticles beginning with the iron phosphides. Although this methodology might, at first blush, appear to be an extension of a well-established procedure, distinct differences are apparent in the chemistry of transition metal pnictide nanoparticle formation in relation to their main group congeners, and attempts to prepare manganese phosphides using similar methodologies have been wholly unsuccessful, as described herein.

The Fe−P phase diagram has a range of stoichiometric compounds including FeP_2, FeP, Fe_2P, and Fe_3P. FeP_2 is a small band gap semiconductor, whereas the FeP phase has a helical ordering of the Fe spins with a net antiferromagnetic interaction at a T_N of 125 K.[16] In contrast, Fe_2P and Fe_3P are both bulk ferromagnets with ordering temperatures of 266 and 716 K, respectively.[15] Although iron phosphide nanoparticles are believed to be responsible for the soft magnetic properties and anti-corrosion behavior in "Ferrophos" coatings,[17] there are no independent reports of the magnetic properties of individual Fe−P phases as discrete nanoparticles.

In this paper we report the synthesis of FeP nanoparticles from $Fe(acac)_3$ and $P(SiMe_3)_3$ as phase-pure, discrete particles of ca. 5 nm in diameter, and the effect of the nanosized dimensions on the resultant magnetic properties. This phase was specially targeted because of the ready accessibility of Fe^{3+} precursors, which makes it an ideal "test case" for oxidation state control in transition metal pnictide nanoparticles, and because it is a major component in Ferrophos alloys. Moreover, nanoparticles of FeP might be expected to exhibit a magnetic behavior similar to that of antiferromagnetic nanoparticles of ferritin[18,19] and NiO,[20,21] which exhibit a permanent moment due to uncompensated spins on the particle surface and superparamagnetic behavior below their Néel temperatures.

Experimental Section

Nanoparticle Synthesis. All manipulations involving transition metal complexes and tris(trimethylsilyl)phosphine were performed in anhydrous reagents under inert atmospheric conditions using argon in a glovebox or on a Schlenk line. Trioctylphosphine oxide (TOPO, Aldrich, 90%), dodecylamine (Acros, 98%), toluene, hexane, methanol, and pyridine (purchased from Fisher) were distilled prior to use. Trioctylphosphine (TOP, Aldrich, 90%), tris(trimethylsilyl)phosphine ($P(SiMe_3)_3$, nitrogen flushed, Acros, 98%), hexylphosphonic acid (HPA, Alfa Aesar), myristic acid (MA, Acros, 95%), manganese(III) acetylacetonate ($Mn(acac)_3$, Aldrich, tech.), manganese(III) 2,2,6,6,-tetramethyl-3,5-heptanedionate ($Mn(TMHD)_3$, Strem, 99%), and iron(III) acetylacetonate ($Fe(acac)_3$, Aldrich, 99%) were used without further purification.

Synthesis of FeP. $P(SiMe_3)_3$ (1.0 mmol) was injected into a 100 °C solution of $Fe(acac)_3$ (1.0 mmol) and dodecylamine (1.0 mmol) or myristic acid (0.4 mmol) in TOPO (25 mL) producing a reddish-orange solution that darkened to black within a few minutes. The temperature was subsequently raised slowly (over a period of hours) to the target temperature (240−320 °C) and the mixture was then allowed to stir for 2−3 d. After 3 d, the reaction mixture was slowly cooled to 80 °C and diluted with ca. 25 mL of pyridine. Pyridine insoluble material (which tended to form at temperatures >260 °C) was separated out, and the nanoparticles were isolated from the filtrate by size-selective precipitation by the addition of aliquots of hexane (∼1 mL), followed by centrifugation and isolation of the supernatant. In some cases, a glovebag under N_2 was used for handling the supernatant and precipitate between centrifugations to avoid surface oxidation of the particles. The resultant greasy black products were subsequently stored in an argon drybox. These reactions were also performed without addition of dodecylamine (DA) or myristic acid (MA), which resulted in the formation of a precipitate, even at 100 °C, and only a small fraction of pyridine soluble nanoparticles. Reactions in which hexylphosphonic acid (HPA, 0.4 or 0.5 mmol) was employed instead of DA or MA resulted in a promising color change, but it was possible to precipitate nanoparticles from the product mixture only when 0.4 mmol was used, and even then the yields were very small.

Synthesis of MnP. Attempts to prepare MnP nanoparticles were conducted by injecting $P(SiMe_3)_3$ (1.0 mmol) into 25 mL of TOPO solutions at 100 °C in which $Mn(acac)_3$ or $Mn(TMHD)_3$ (1.0 mmol) was dissolved. As for FeP, the temperature was raised to 260−300 °C with continuous stirring. The initial deep red solution darkened upon phosphine addition, but never turned black, even after stirring for 3−5 d at 300 °C. Attempts to precipitate nanoparticles from the resultant solutions were unsuccessful.

Chemical Analysis. Chemical analyses were performed by RTI Laboratories, Livonia, MI. Samples were prepared by dissolving dried nanocrystals in 50% (by volume) nitric acid aqueous solutions. The yield of particles was based on the total quantity of Fe precipitated from solution as nanoparticles relative to the quantity of Fe used in the synthesis: 214 ppm aqueous solution of nanoparticles, $Fe_{calc} = 53$ ppm, and $Fe_{obs} = 45$ ppm. TOPO coverage was calculated from the excess phosphorus within the second precipitated fraction that could not be attributed to FeP: 222 ppm solution of FeP nanoparticles, $Fe_{obs} = 57$ ppm, $P_{obs} = 36$ ppm, $P_{calc(FeP)} = 31.6$ ppm.

X-ray Diffraction. Powder X-ray diffraction patterns were collected on a Rigaku Ru200B 12 kW diffractometer using Cu Kα radiation (1.54056 Å) at 40 kV and 150 mA. Samples were prepared by pressing powders at 4000 psi to form pellets and affixing them to quartz (*0001*) low background holders.

Transmission Electron Microscopy. Imaging was carried out with a medium-sized objective aperture on a JEOL 2010F electron microscope (University of Michigan − EMAL) operating at 200 kV. Samples were prepared by depositing a few drops of a pyridine solution of nanoparticles (∼mM concentration) onto 300-mesh TEM Cu grids coated with thin amorphous carbon films (SPI Supplies). Energy-dispersive spectroscopy (EDS) was used to confirm the presence of iron and phosphorus in the imaged particles.

Magnetic Measurements. Magnetic studies were performed using a Quantum Design MPMS-5S SQUID magnetometer in the Department of Physics, Wayne State University. To ensure no field-induced movement of the powder, samples were mixed with a resin (Eicosain) prior to sealing under vacuum within quartz sample tubes.

(16) Felcher, G. P.; Bellavance, D.; Wold, A.; Smith, F. A. *Phys. Rev. B* **1971**, *3*, 3046−3052.
(17) Zećević, S. K.; Zotović, J. B.; Gojković, S. L.; Radmilović, V. *J. Electroanal. Chem.* **1998**, *448*, 245−252.
(18) Makhlouf, S. A.; Parker, F. T.; Berkowitz, A. E. *Phys. Rev. B* **1997**, *55*, R14717−R14720.
(19) Seehra, M. S.; Punnoose, A. *Phys. Rev. B* **2001**, *64*, 132410−132413.
(20) Makhlouf, S. A.; Parker, F. T.; Spada, F. E.; Berkowitz, A. E. *J. Appl. Phys.* **1997**, *81*, 5561−5563.
(21) Kodama, R. H.; Makhlouf, S. A.; Berkowitz, A. E. *Phys. Rev. Lett.* **1997**, *79*, 1393−1396.

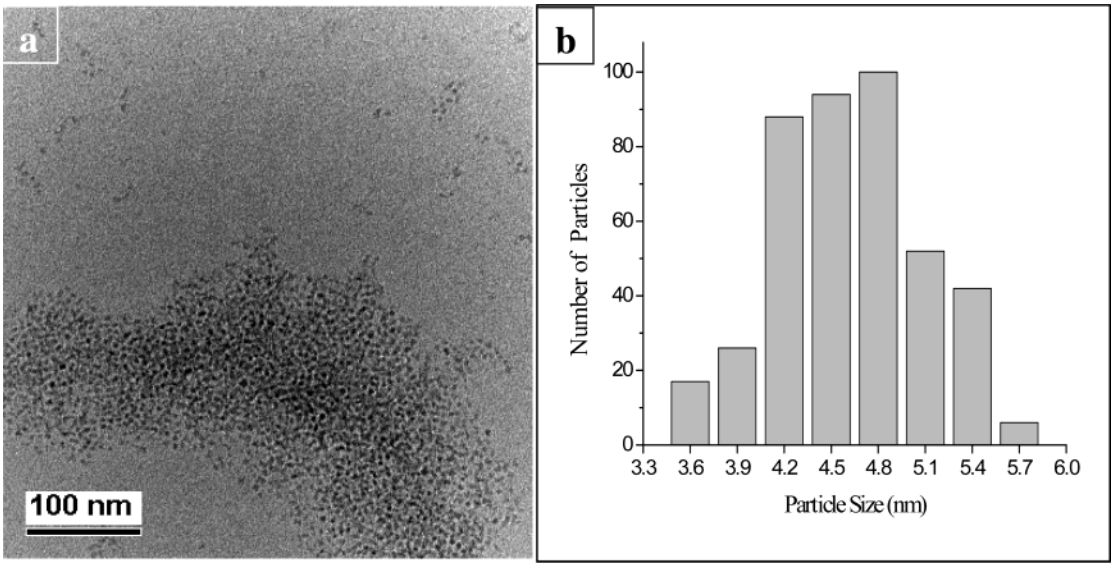

Figure 1. (a) TEM micrograph showing FeP nanoparticles synthesized using DA as the capping agent at 260 °C (×40 K). (b) Size distribution histogram ($N = 425$; average size = 4.65 ± 0.74 nm).

Results and Discussion

Synthesis of FeP Nanoparticles. The synthesis of III−V based semiconductor nanoparticles using metathesis reactions at elevated temperatures is well established.[22] The important features are the use of a high boiling solvent (so that samples can be annealed at moderate temperatures, $T < 350$ °C) and the presence of coordinating capping groups to prevent aggregation. Commonly, trioctylphosphine (TOP) or trioctylphosphine oxide (TOPO) is used to satisfy both of these requirements. In some cases, a second capping agent, such as dodecylamine (DA), myristic acid (MA), or hexylphosphonic acid (HPA), is added. These secondary capping agents are employed in-situ for particle shape and size control[23] and/or to alter the solubility and air-sensitivity of the resultant particles.[24] Under long annealing times, a range of particle sizes can be produced,[9] and these can be separated via size-selective precipitation techniques or size-exclusion chromatography.

In our investigation, we started by exploring parameters reported to be successful for InP.[9] The most common method (as well as the one reported to give the narrowest size distributions) involves dissolution of the metal salt or complexes in TOP, followed by injection into TOPO at high temperature. However, the low solubility of $Fe(acac)_3$ in TOP precluded this pathway. Accordingly, FeP nanoparticles were produced by injecting the phosphine source, $P(SiMe_3)_3$, into a solution of $Fe(acac)_3$ dissolved in TOPO, and heated at 100 °C. Upon injection, the solution immediately turned red, then darkened quickly to black. Subsequently, a fine black precipitate formed within 10 min of the injection. This was then heated at a range of temperatures (240−320 °C); however, above 280 °C a black crust was observed to form on the sides of the flask. This crusty black precipitate constituted the major product and resisted dissolution in all common solvents. To avoid precipitation, the reaction was carried out with secondary capping groups. The addition of ligands such as MA (Fe/MA = 1:0.4 mol) or DA (Fe/DA = 1:1 mol) to the reaction produced transparent solutions and resulted in the formation of nanoparticles that are pyridine-soluble. Attempts to perform size-selective precipitation typically resulted in only two fractions, even when very small aliquots of MeOH or hexane (precipitating agent) were added. As was also reported for InP, the first fraction is inevitably contaminated by a reaction byproduct and is therefore discarded.[9] If left in air or washed with methanol, precipitated particles lose their solubility entirely, presumably due to surface oxidation or loss of capping group.[9]

The size distribution of DA-capped nanoparticles was determined by measuring particle sizes directly from TEM images (Figure 1). Most of the nanoparticles were found to be spherical and show a narrow size distribution with an average particle size of 4.65 ± 0.74 nm (±16% standard deviation). EDS confirmed the presence of iron and phosphorus in the imaged particles.

The identity of the particles was confirmed by X-ray powder diffraction (XRD) (Figure 2). For DA or MA capped nanoparticles, broad humps are evident in the 2θ regions of 30−40°, 45−50°, and 50−60°, which are consistent with expected peak groupings for FeP. Furthermore, the breadth of the peaks is in harmony with the small coherence length expected for a nanoparticulate phase. Although the Scherrer formula could not be employed for crystallite size determination in these samples because of peak overlap, estimates of the expected peak broadening are consistent with particle sizes on the order of 5 nm for $Fe(acac)_3$ (Table 1) and compare favorably to the values obtained by TEM. Attempts to match observed peak envelopes to those of other iron phosphide (i.e., FeP_2, Fe_2P, Fe_3P) or phosphate phases were unproductive, indicating that the redox neutral de-silylation strategy has been successful in the production of phase-pure FeP nanoparticles.

(22) Green, M. *Curr. Opin. Solid State Mater. Sci.* **2002**, *6*, 355−363.
(23) Manna, L.; Scher, E. C.; Alivisatos, A. P. *J. Am. Chem. Soc.* **2000**, *122*, 12700−12706.
(24) Meulenberg, R. W.; Strouse, G. F. *J. Phys. Chem. B* **2001**, *105*, 7438−7445.

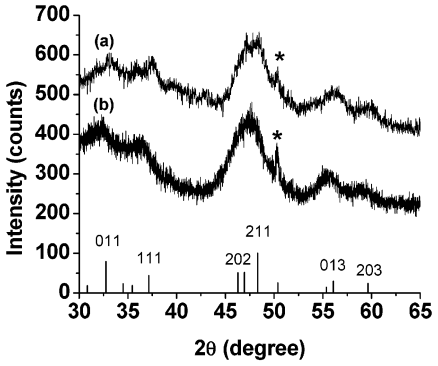

Figure 2. Powder X-ray diffraction spectrum of FeP nanoparticles synthesized using (a) Fe/dodecylamine (1:1 mol) at 260 °C, and (b) Fe/myristic acid (1:0.4 mol) at 250 °C. The line diagram illustrates the positions and relative intensities for reflections of FeP (JCDPS 39-0809), with major reflections indexed. The (∗) denotes a background peak from the sample holder.

Table 1. Calculated Full Width at Half-Maximum (FWHM) Values as a Function of Nanoparticle Size for Diffraction from the (211) Plane ($\theta = 24.16°$) Based on the Scherrer Equation[a]

particle size (nm)	FWHM (degrees)
1	8.711
5	1.742
10	0.871

[a] $t = (0.9\lambda)/(B\cos\theta_B)$; where t is the particle size (Å), λ is the wavelength of X- rays (Cu Kα = 1.54056 Å), B = FWHM (rad), and θ_B is the angle of the peak (rad). Ref 28.

Chemical analysis data are also consistent with the formulation FeP. For nanoparticles prepared in the presence of DA, the ratio of Fe/P obtained from ICP is 1:1.14. It is well established that particles precipitated from TOPO/ligand mixtures inevitably have both capping groups adhered to their surface; therefore, we attribute the excess phosphorus (12 mol %) to the presence of TOPO groups partially capping the surface of the nanoparticles. This interpretation is also consistent with data obtained from X-ray photoelectron spectroscopy (XPS). The high-resolution spectrum of the P $2p_3$ region shows two peaks: one at 128.3 eV that can be assigned to FeP (P^{3-}) and the other at 131.6 eV corresponding to oxidized phosphorus due to TOPO and any on oxidation of the nanoparticle surfaces (Supporting Information). The relative peak areas (70:30 for P^{3-}/P^{n+}) are also consistent with the majority phase in our samples being FeP.

Interestingly, although the use of strong binding ligands such as hexylphosphonic acid (HPA) resulted in a promising color change when employed with TOPO, it yielded only small quantities of precipitated particles, and only when lesser molar concentrations of HPA were employed (0.4 mmol vs 0.5 mmol). The diffraction patterns of these samples were diffuse, although features suggestive of FeP were present (Supporting Information). These data are consistent with the production of very small crystallites (ca. 1 nm) as estimated from peak broadening in the XRD, and/or formation of amorphous particles. Thus, it would appear that there is an optimal ligand binding strength for production of FeP nanoparticles with the desired attributes. TOPO itself does not bind strongly enough, which results in rapid nucleation followed by aggregation of particles (as it is a chelating agent, the acetylacetonate actually acts to moderate the nucleation when $Fe(acac)_3$ is used; reactions with $FeCl_3$ in TOPO produce smaller particles and a greater degree of aggregation[25]). HPA perhaps binds too well, preventing condensation reactions and the production of sizable nanoparticles, or acting to disrupt the crystallization process, resulting in amorphous product. DA and MA, on the other hand, are near optimal, resulting in uniform particles with excellent solubility properties that can be recovered by precipitation in high yields (85%, based on amount of iron consumed).

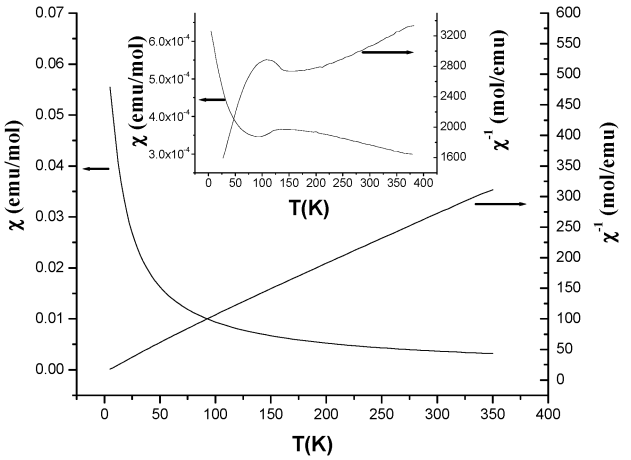

Figure 3. Temperature dependence of molar susceptibility (χ) and inverse molar susceptibility (χ^{-1}) for 5-nm FeP nanoparticles synthesized using DA as the capping agent at 260 °C, and bulk FeP (inset), for H = 3.0 T.

The fact that the particles produced are so uniform in size implies that nucleation and condensation are achieved *upon mixing* at 100 °C, and the role of annealing times serves only to improve crystallinity. This is consistent with the rapid color change (minutes) observed upon injection, and suggests a greater reactivity for Fe^{3+} relative to main group analogues. Temperature is certainly a critical parameter for the formation of well-crystallized samples, and annealing temperatures of at least 240 °C are required. However, the increased reactivity of Fe is also manifested as an increased tendency to aggregate, resulting in precipitate formation in samples heated at >260 °C. Overall, this methodology has the advantage of forming narrow polydispersity samples of reproducible size (∼5 nm). Furthermore, formation of larger particles is likely to be feasible if multiple injections of reagents are employed in the synthesis.[26]

Magnetic Properties of FeP Nanoparticles. To probe the effect of nanoscale dimension on the magnetic properties, the temperature-dependent magnetic susceptibility was measured on both bulk and nanoparticulate FeP (Figure 3). The susceptibility of bulk FeP synthesized in our lab follows a Curie−Weiss behavior (i.e., the inverse molar susceptibility, χ^{-1}, varies linearly with temperature) above ∼200 K with an effective magnetic moment (μ_{eff}) of 1.59 μ_B per Fe atom. At 120−125 K, an antiferromagnetic transition (T_N) onset is

(25) Perera, S. C.; Brock, S. L. *Mater. Res. Soc. Symp. Proc.* **2003**, *755*, DD5.9.1−DD5.9.6.
(26) Xiaogang, P.; Wickham, J.; Alivisatos, A. P. *J. Am. Chem. Soc.* **1998**, *120*, 5343−5344.

observed. These results are consistent with previously published results[16,27] on bulk FeP (μ_{eff} of 1.83 μ_B per Fe above 300 K, T_N near 120 K). Neutron diffraction measurements[16] have shown that the magnetic ordering in this material is not simple: FeP has a complex helimagnetic structure below about 125 K in which the spins are ordered in a parallel fashion within the *ab* plane, but rotate in the *c* plane over a period of 5 unit cells (~2.9 nm) resulting in a net antiferromagnetic alignment.

In contrast to the bulk system, the FeP nanoparticles that we have produced behave paramagnetically, exhibiting a Curie−Weiss behavior down to ~75 K with no discernible magnetic ordering temperature and with a larger effective moment of 2.98 μ_B per Fe atom (Figure 3). Although this moment is substantially smaller than the expected spin-only value of 5.9 μ_B for Fe^{3+}, it is nearly double that of bulk FeP. The linear extrapolation of the high-temperature χ^{-1} vs T data for the FeP nanoparticles yields a small negative Curie−Weiss temperature ($\theta = -28$ K), indicating an antiferromagnetic coupling between the Fe spins in each nanoparticle. Below ~75 K, χ^{-1} begins to deviate away from the linear extrapolation and toward the origin. This behavior is consistent with some of the Fe spins within each nanoparticle becoming antiferromagnetically (or helically) ordered, at least over a short range, which would yield a smaller effective moment per Fe atom (larger χ^{-1} slope), and with these FeP nanoparticles themselves behaving as noninteracting particles (Curie-like behavior with zero intercept). Furthermore, no discernible hysteretic behavior was observed between the experimentally measured zero-field-cooled (ZFC) and field-cooled (FC) magnetic susceptibilities for our FeP nanoparticle samples, even for fields as low as 0.010 T.

This behavior can be compared to that observed in a number of antiferromagnetic nanoparticle systems, including NiO[20,21] and ferritin,[18,19] in which the nanoparticles exhibit permanent moments below their Néel temperatures. This finite moment can be understood in terms of uncompensated spins on the particle surface, in accordance with the model put forth by Néel.[27] Moreover, superparamagnetism results from the spin fluctuation of these nanoparticle moments. These superparamagnetic particles typically freeze into a fixed orientation or direction at some temperature T_B, characterized by a bifurcation between the ZFC and FC magnetization data, as the moments are not free to align with the field within the measuring time for $T < T_B$ after zero-field cooling. Because no discernible magnetic hysteretic behavior was observed for our FeP nanoparticles, this suggests that the comparable size of the actual FeP nanoparticles (~5 nm) to the magnetic cell *c*-dimension (~2.9 nm) might preclude the onset of long-range helical antiferromagnetical order within the nanoparticles and the appearance of an archetypal superparamagnetic behavior.

Application to Other Transition Metals. Attempts to prepare MnP from manganese(III) acetylacetonate ($Mn(acac)_3$) via the same route have proven to be unsuccessful. Although there was a clear color change from red to a deep red upon the injection of phosphine to Mn/TOPO solutions, the color did not change any further, regardless of the heating conditions. More problematically, it was never possible to isolate any product from the resultant solution. Because of concerns about the purity of the acac (with specific concerns about water), we also explored reactions with a higher purity (99%) precursor, manganese(III) 2,2,6,6-tetramethyl-3,5-heptanedionate ($Mn(TMHD)_3$), with the same results. We attribute the apparent lack of reactivity to oxophilicity on the part of trivalent manganese. Indeed, attempts to react $Mn(acac)_3$ with $P(SiMe_3)_3$ in more conventional solvents (e.g., acetonitrile) at moderate temperatures produced amorphous precipitates that had Mn, but no P, suggesting that reaction between these species is not facile. Thus, we conclude that regardless of the apparent simplicity of the method, the variation in chemical behavior of different metals must be taken into account when designing de-silylation strategies for production of metal phosphide nanoparticles.

Conclusions

In summary, application of de-silylation strategies to transition metal pnictide syntheses has successfully been employed for the production of ca. 5-nm diameter phase-pure FeP nanoparticle samples with relatively narrow polydispersity (~16% standard deviation). The magnetic behavior of FeP nanoparticles is unique from that of bulk FeP (antiferromagnetic order below 124 K) as no transition to long-range order is observed down to 5 K. This is undoubtedly due to the small diameter of the particles, which is on the order of the magnetic cell dimensions in these materials (~2.9 nm). Current research is focused on developing new synthetic routes that will permit the control of a broader range of particle sizes, and which can be successfully extended to other transition metal pnictides.

Acknowledgment. This work is supported by an NSF-CAREER award (DMR-0094273) and the Institute for Manufacturing Research at Wayne State University. The microscopy was performed at the University of Michigan EMAL on the JEOL 2010F, which was purchased under NSF grant DMR-9871177. We thank John Mansfield and Corinna Wauchope (University of Michigan-EMAL) for their assistance with TEM and XPS studies.

Supporting Information Available: A figure of the X-ray photoelectron spectroscopy data obtained for FeP nanoparticles and a figure of the X-ray powder diffraction pattern obtained for FeP nanoparticle synthesis with HPA (0.4 mmol) (PDF). This material is available free of charge via the Internet at http://pubs.acs.org.

CM034443O

(27) Néel, L. In *Low-Temperature Physics*; DeWitt, C., Dreyfus, C., DeGennes, P. G., Eds.; Gordon and Breach: New York, 1962; p 413.
(28) Cullity, B. D. *Elements of X-ray Diffraction*, 2nd ed.; Addison-Wesley: Reading, MA, 1978; p 102.